Journal of Organometallic Chemistry, 461 (1993) 187–199

JOM 23733

A Mössbauer effect and Fenske–Hall molecular orbital study of the bonding in a series of organoiron–copper clusters

Margaret L. Buhl and Gary J. Long [1]

Department of Chemistry, University of Missouri-Rolla, Rolla, MO 65401 (USA)

G. Doyle

Geo-Centers, Inc., Lake Hopatcong, NJ 07849 (USA)

(Received November 30, 1992; in revised form March 22, 1993)

Abstract

The electronic properties of a series of organoiron-copper clusters, $Na_2[Cu_6Fe_4(CO)_{16}]$ (**I**), $Na_3[Cu_5Fe_4(CO)_{16}]$ (**II**), $Na_3[Cu_3Fe_3(CO)_{12}]$ (**III**), $[Cu(P(CH_3)_3)_4]_2[Fe_3(CO)_{12}Cu_4(P(CH_3)_3)_2]$ (**IV**), $[((C_6H_{11})_3PCu)_2Fe(CO)_4]$ (**V**), $[((Ph_3P)_2Cu)_2Fe(CO)_4]$ (**VI**), $[(Ph_3P)_2CuFe(CO)_3(NO)]$ (**VII**), and $[((NH_3)_2Cu)_2Fe(CO)_4]$ (**VIII**), have been investigated experimentally by the Mössbauer effect and theoretically by Fenske–Hall molecular orbital calculations. The Mössbauer effect hyperfine parameters are sensitive to the variety of bonding situations found in these clusters. The Mössbauer effect isomer shifts observed for these clusters range from −0.141 to −0.037 mm/s at 78 K. The expected increase in the isomer shift with a decrease in the iron 4s Mulliken atomic orbital population, and a decrease in the Clementi effective nuclear charge experienced by the iron 4s electrons is observed. The electric field gradients at the iron sites have been calculated and compared with the experimental quadrupole splittings which range from 0.191 to 2.497 mm/s at 78K. The valence contribution was found to be the major component of the electric field gradient and is directly related to the symmetry of the iron electronic environment. The calculated values of the electric field gradients are also used to confirm the Mössbauer effect spectral assignments in **II**. The calculated metal–metal bond energy decreases as the cluster metal–metal bond length increases. The major bonding in these clusters is the iron–copper bond in which the iron 3d atomic orbitals overlap the copper 4s and 4p atomic orbitals.

1. Introduction

It is well known that organometallic clusters play an important role in surface studies during the processes of chemisorption and catalysis [1]. A further understanding of these processes may be obtained from studies of the electronic properties of organometallic clusters [2,3]. Mixed metal organometallic clusters are especially interesting because they can provide useful precursors when catalysts of well defined mixed-metal composition are required. In this work, the electronic properties of several unique organoiron–copper compounds have been investigated through the study of their Mössbauer effect hyperfine parameters and the calculation of their electronic properties. The organoiron-copper clusters considered [4–7] in this work are the anionic clusters, $Na_2[Cu_6Fe_4(CO)_{16}]$ (**I**), $Na_3[Cu_5Fe_4(CO)_{16}]$ (**II**), $Na_3[Cu_3Fe_3(CO)_{12}]$ (**III**), and $[Cu(P(CH_3)_3)_4]_2[Fe_3(CO)_{12}Cu_4(P(CH_3)_3)_2]$ (**IV**), shown schematically in Fig. 1, and the neutral clusters, $[((C_6H_{11})_3PCu)_2Fe(CO)_4]$ (**V**), $[((Ph_3P)_2Cu)_2Fe(CO)_4]$ (**VI**), $[(Ph_3P)_2CuFe(CO)_3(NO)]$ (**VII**), and $[((NH_3)_2Cu)_2Fe(CO)_4]$ (**VIII**).

The copper atoms in each of the anionic clusters, **I–IV**, serve to bridge the $Fe(CO)_4$ groups, either in a coplanar edge-like fashion, as in **II**, **III**, and **IV**, in which the iron is coordinated with either two or three copper atoms, or in a facial fashion, as in **I** and **IV**, in which the iron is coordinated with three copper atoms. As a result, cluster **I** has an octahedron of copper atoms whose alternate trigonal faces are capped with $Fe(CO)_4$ groups. In contrast, the iron and copper atoms

Correspondence to: Professor G.J. Long.

[1] Address until August 1994: Institut de Physique B5, Université de Liège, B-4000 Sant-Tilman, Belgium.

0022-328X/93/$6.00

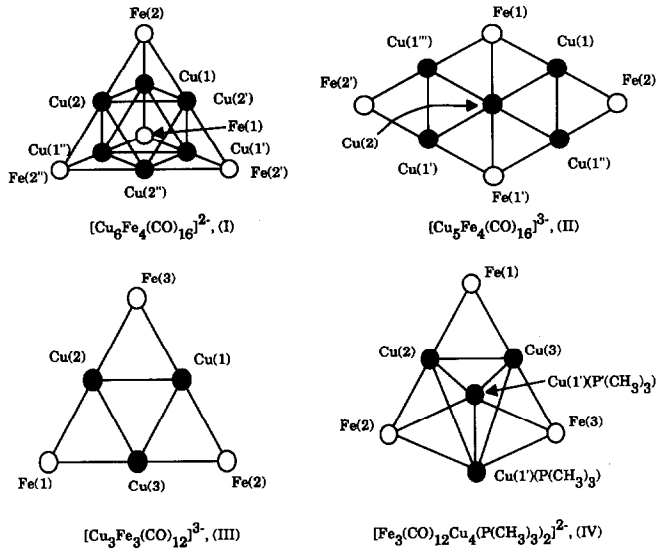

Fig. 1. Schematic structures of the anionic clusters.

in **II** and **III** are nearly planar, and **IV** has a tetrahedron of copper atoms with one $Fe(CO)_4$ bonded to an edge and two $Fe(CO)_4$ groups bonded to two faces. Because the X-ray structure [7] of **VII** reveals that the three carbonyl and one nitrosyl ligands are completely disordered, one of the two iron to copper bridging ligands may be a nitrosyl ligand. These unique structures, as well as the other neutral clusters, provide a unique opportunity to study the electronic properties of metal clusters in a variety of geometries.

The anionic clusters **I**, **II**, and **III** have been found to interconvert in solution depending on the amount of copper(I) halide or $Na_2Fe(CO)_4$ added to the solution [5,7]. Although the mechanisms for the transformations are not known, it is thought that the original cluster undergoes at least partial fragmentation which subsequently leads to the formation of the new cluster.

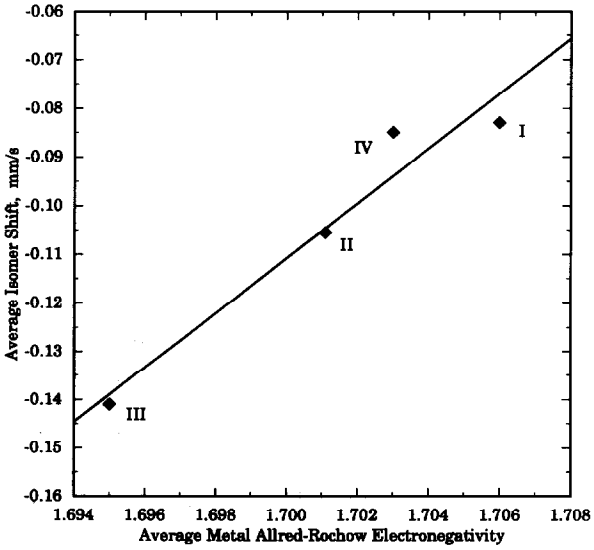

Fig. 2. The average isomer shift *vs.* the average Allred–Rochow electronegativity of the metal atoms.

In our preliminary report on the Mössbauer spectra of these organoiron-copper clusters, we found that an increase in the ratio of the anionic cluster charge to the number of iron atoms was linearly related to an increase in the isomer shift. Perhaps more useful, it was also found that the average Allred–Rochow electronegativity of the metal atoms in the cluster was related linearly to the isomer shift, as is shown in Fig. 2. Because copper is more electronegative than iron, a larger number of copper atoms leads to a larger average Allred–Rochow metal electronegativity. The increased tendency to attract electron density toward the copper atoms decreases the s-electron density at the iron nucleus and results in a larger isomer shift.

In several related studies [3,8–11], we have shown that Fenske–Hall molecular orbital calculations are helpful in providing insight into the electronic distributions within organoiron clusters and in making Mössbauer effect spectral assignments. Although the Fenske–Hall molecular orbital calculations presented here are less helpful in making the Mössbauer effect spectral assignments, the calculations do provide insight into the electron density distributions. The molecular orbital wave function coefficients and the resulting Mulliken atomic charges have been used both to relate, through the Clementi and Raimondi effective nuclear charge, the electron density to the isomer shift, and to calculate the electric field gradients at the iron sites in the clusters. A comparison of the iron 4s Mulliken population, the effective nuclear charge, and the calculated quadrupole splittings with the experimental Mössbauer effect hyperfine parameters provides verification of the iron electronic densities determined by the molecular orbital calculations.

2. Experimental section

The clusters were prepared and characterized and were the same samples as reported upon previously [4–7]. The Mössbauer effect absorbers were prepared in a nitrogen atmosphere in a Vacuum Atmospheres Co. inert atmosphere box. The Mössbauer effect spectra were obtained at 78K on a conventional constant accceleration spectrometer which utilized a room temperature rhodium matrix cobalt-57 source and was calibrated at room temperature with natural abundance α-iron foil. The spectra were fit to symmetric Lorentzian doublets with equal line widths by using standard least-squares computer minimization tech-

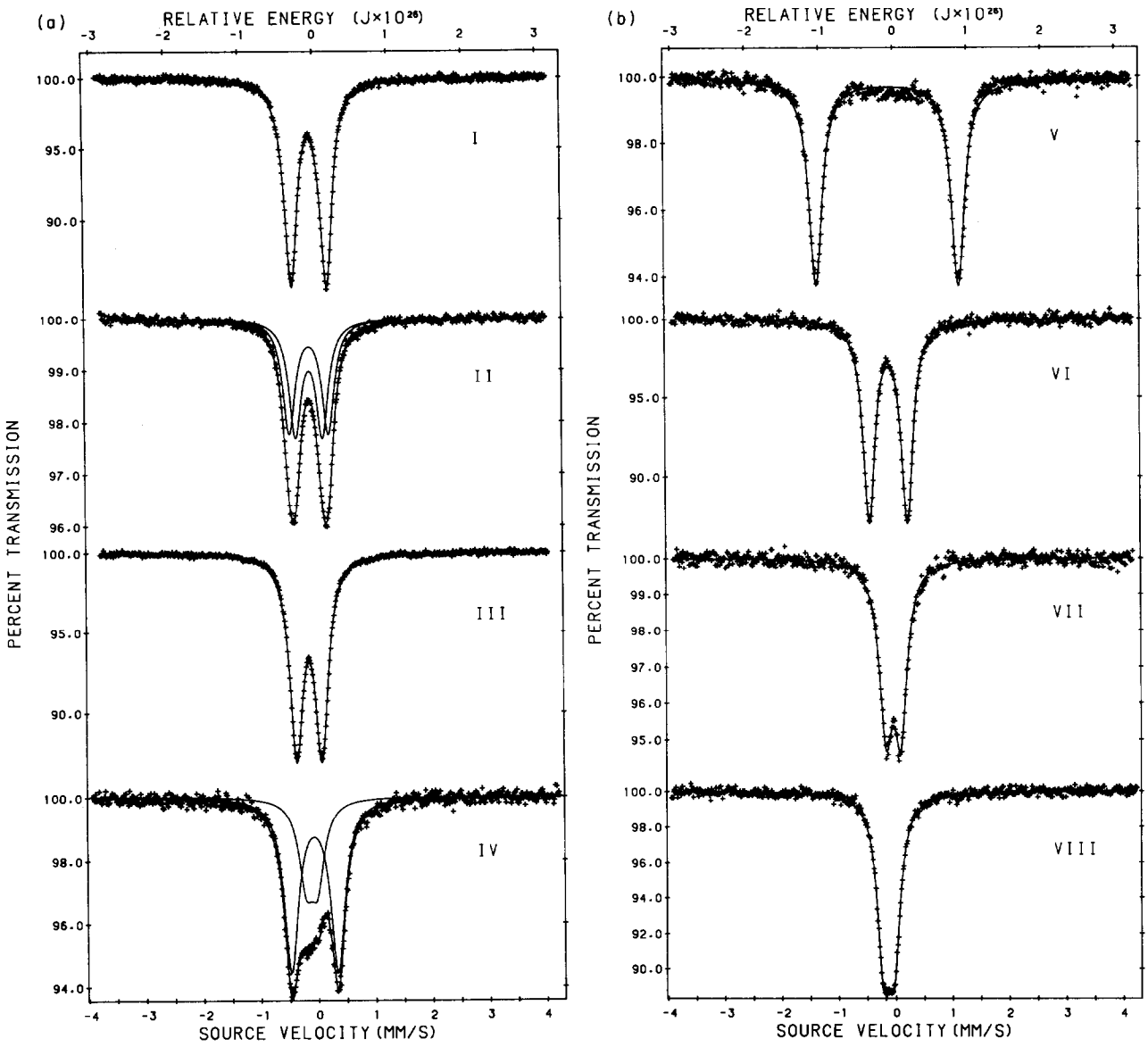

Fig. 3. Mössbauer effect spectra of clusters I–IV (A) and V–VIII (B) obtained at 78 K.

niques. The typical error limits are ±0.005 mm/s for the isomer shifts, ±0.01 mm/s for the quadrupole splittings and the line widths, and at most ±1% for the areas.

The molecular orbital calculations were performed by using the FENSKE–HALL molecular orbital program [12] and atomic positions derived from the X-ray structures of these compounds [5,7,13*]. The calculations were performed by using the Herman–Skillman [14] atomic basis functions as modified with the Xα to Slater basis program of Bursten and Fenske [8,15,16*]. This basis set was used for all the calculations reported in this work. A Mulliken population analysis was used to determine the atomic orbital occupancy factors and the atomic charges. After considering the structural approximations discussed below and the basis set approximations, the typical error limits for the absolute metal charges are estimated [17] to be ±0.06. The typical error limits for the absolute carbonyl and phosphine ligand charges and for the metal atomic orbital populations are estimated to be ±0.15 or better. The relative error for a series of compounds are estimated to be a factor of three smaller. A more extensive discussion concerning the error limits of the results of the Fenske–Hall molecular orbital calculations is pre-

* Reference number with asterisk indicates a note in the list of references.

sented elsewhere [17]. The atomic charges were used to calculate [17] the lattice contribution to the electric field gradient at the iron nucleus. The Fenske–Hall derived iron wave functions were used to calculate [17] the valence contribution to the electric field gradient. The expectation values, $\langle r^{-3}\rangle_{3d}$ and $\langle r^{-3}\rangle_{4p}$, for iron were calculated from the 3d Mulliken orbital populations, whereas those for the copper were held at the constant values of 32.0 for $\langle r^{-3}\rangle_{3d}$ and 11.6 for $\langle r^{-3}\rangle_{4p}$ [18–20].

The structures used for the Fenske–Hall molecular orbital calculations of clusters **V** and **VI** were approximated [17] from their X-ray structures. The tricyclohexylphosphine ligands in cluster **V** were replaced with phosphine ligands in which the phosphorus to hydrogen distance was 1.48 Å, the distance found in phosphine. Nine of the twelve phenyl rings in cluster **VI** were also replaced with hydrogen atoms at a phosphorus to hydrogen distance of 1.48 Å, the distance found in phosphine.

The Fenske–Hall molecular orbital calculations were performed by using the transform basis method. The iron and the copper fragments were formed by combining the metal atom with the corresponding ligand fragments, both in their correct spacial arrangement. The resulting iron and copper fragments were then combined to form the molecule. The total occupied molecular orbital energy, E_T, is given by

$$E_T = \sum_i n_i E_i \qquad (1)$$

where the summation is over all i occupied molecular orbitals, n_i is the number of electrons per occupied molecular orbital, usually two, and E_i is the energy of the occupied molecular orbital. In our Fenske–Hall transform basis calculations [17], only iron–copper bonds are formed when the final fragments of a cluster are combined. The resulting cluster bond energy, E_{BE}, the energy released upon formation of the cluster from its fragments, is the total iron-copper bond energy and is given by

$$E_{BE} = \left[\sum_f n_f E_f\right] - E_T \qquad (2)$$

where the summation is over all f occupied fragment orbitals, n_f is the number of electrons per occupied fragment orbital, usually two, and E_f is the energy of the occupied fragment orbital. When the total iron-copper bond energy is divided by the number of iron–copper bonds formed, the iron–copper bond energy per iron–copper bond is obtained.

3. Results and discussion

3.1. Mössbauer effect spectra

The Mössbauer effect spectra for the organoiron–copper clusters are shown in Fig. 3, and the derived spectral parameters are given in Table 1. When fitting these spectra, a distinction is made in a cluster between chemically equivalent iron sites and crystallographically equivalent iron sites. Chemically equivalent iron sites have the same chemical environment in that they have the same kind and number of coordinated atoms and have similar bond lengths and angles. Crystallographically equivalent iron sites in a cluster have atomic positional coordinates which are related by a symmetry transformation that belongs to the crystallographic space group of the cluster. The Mössbauer effect is typically able to distinguish between chemically non-equivalent iron sites, but is not necessarily able to distinguish between crystallographically non-equivalent, but chemically equivalent, iron sites. All of

TABLE 1. Mössbauer effect spectral parameters [a]

Cluster	Site	T (K)	δ	ΔE	Γ	% area
$Na_2[Cu_6Fe_4(CO)_{16}]$ (**I**)		295	−0.153	0.606	0.26	100
		78	−0.082(5)	0.617(5)	0.26(1)	100
$Na_3[Cu_5Fe_4(CO)_{16}]$ (**II**)	Fe(1)	295	−0.192	0.654	0.28	50 [a]
	Fe(2)	295	−0.167	0.497	0.28	50 [b]
	Fe(1)	78	−0.107(6)	0.683(9)	0.26(1)	50 [b]
	Fe(2)	78	−0.105(6)	0.472(9)	0.26(1)	50 [b]
$Na_3[Cu_3Fe_3(CO)_{12}]$ (**III**)		295	−0.211	0.414	0.28	100
		78	−0.141(5)	0.442(5)	0.28(1)	100
$[Cu(P(CH_3)_3)_4]_2[Fe_3(CO)_{12}Cu_4(P(CH_3)_3)_2]$ (**IV**)	Fe(1)	78	−0.118	0.200	0.30	32.7
	Fe(2,3)	78	−0.069	0.815	0.30	67.3
$((C_6H_{11})_3PCu)_2Fe(CO)_4$ (**V**)		78	−0.129	0.191	0.26	100
$((Ph_3P)_2Cu)_2Fe(CO)_4$ (**VI**)		78	−0.095(6)	2.497(1)	0.28(1)	100
$(Ph_3P)_2CuFe(CO)_3(NO)$ (**VII**)		78	−0.037(6)	0.261(1)	0.28(1)	100
$((NH_3)_2Cu)_2Fe(CO)_4$ (**VIII**)		78	−0.103(5)	0.668(7)	0.25(1)	100

[a] Spectral parameters are given in mm/s with the isomer shifts relative to room temperature natural abundance α-iron foil. [b] Area constrained to the value given.

TABLE 2. Fenske–Hall derived cluster energies

Cluster	HOMO-LUMO gap (eV)	E_T (eV)	E_{BE} (eV)	Number of bonds formed		E_{BE}/bond (eV)	Average bond distance (Å)	
			Fe–Cu	Fe–Cu	Cu–Cu	Fe–Cu	Fe–Cu	Cu–Cu
$[Cu_6Fe_4CO)_{16}]^{2-}$ (I)	4.21	−3370	42.7	12	12	3.56	2.46	2.62
$[Cu_5Fe_4CO)_{16}]^{3-}$ (II)	4.11	−2410	37.8	10	6	3.77	2.43	2.53 [a]
								2.69 [b]
$[Cu_3Fe_3CO)_{12}]^{3-}$ (III)	4.50	−1540	23.8	6	3	3.97	2.41	2.60
$[Fe_3(CO)_{12}Cu_4(P(CH_3)_3)_2]^{2-}$ (IV)	2.92	−3120	23.6	8	6	2.94	2.42 [c]	2.41 [e]
							2.69 [d]	2.77 [f]
								2.48 [g]
$((C_6H_{11})_3PCu)_2Fe(CO)_4$ (V)	5.66	−1480	11.5	2	–	5.73	2.34	–
$((Ph_3P)_2Cu)_2Fe(CO)_4$ (VI)	2.41	−3620	6.7	2	–	3.34	2.51	–
$(Ph_3P)_2CuFe(CO)_3(NO)$ (VII)	4.22	−5350	2.3	1	–	2.32	2.59	–

[a] The average of the Cu(2)–Cu(1, 1″,1‴) bond distances. [b] The average of the Cu(1)–Cu(1″) and Cu(1′)–Cu(1‴) bond distances. [c] The average of the Fe(1)–Cu(2,3) bond distances. [d] The average of the Fe(2,3)–Cu(1,1′,2,3) bond distances. [e] The Cu(1)–Cu(1′) bond distance. [f] The average of the Cu(1)–Cu(2,3) bond distances. [g] The Cu(2)–Cu(3) bond distance.

the fits shown in Fig. 3 and reported in Table 1, are consistent both with these criteria and with the degeneracy expected for a specific site.

The structures and the Mössbauer spectra of the clusters I–IV indicate that the iron sites with facial bonding have less negative isomer shifts than do the iron sites with edge bonding. For the facial bonding found in I and IV, the isomer shifts are −0.083 and −0.069 mm/s, respectively, whereas for the edge bonding found in II–IV, the isomer shifts range from −0.105 to −0.141 mm/s. In II, the Fe(2) site has a chemical environment which is similar to that in III in which the iron atom is bonded in an edge-like fashion to two copper atoms. Similarly, in cluster II, Fe(1) is bonded in an edge-like fashion to three copper atoms. Because a poor fit was obtained when the Mössbauer spectrum of cluster II was fit with one symmetric quadrupole doublet, two symmetric quadrupole doublets with similar isomer shifts, but different quadrupole interactions, were used. Based on a comparison of the quadrupole splittings, the inner quadrupole doublet was assigned to Fe(2) and the outer quadrupole doublet was assigned to Fe(1) (see Table 1). The neutral molecules each have a single iron

TABLE 3. Cluster Mulliken atomic populations, charges, and effective nuclear charges

Cluster	Site	Avg. Mulliken atomic population				Atomic charge		Avg Z_{eff} [a]	Avg Z_{eff} [b]
		3d	4s	4p	Total	Metal	Avg. CO		
$[Cu_6Fe_4(CO)_{16}]^{2-}$ (I)	Fe	6.72	0.42	1.10	8.24	−0.24	−0.14	3.11	4.76
	Cu	9.80	0.80	0.21	10.80	0.20		3.80	5.22
$[Cu_5Fe_4(CO)_{16}]^{3-}$ (II)	Fe(1)	6.71	0.44	1.09	8.24	−0.24	−0.15	3.11	4.76
	Fe(2)	6.75	0.42	1.16	8.33	−0.33	−0.17	3.06	4.72
	Cu(1)	9.82	0.83	0.22	10.87	0.14		3.78	5.20
	Cu(2)	9.79	0.81	0.24	10.84	0.16		3.79	5.22
$(Cu_3Fe_3(CO)_{12}]^{3-}$ (III)	Fe	6.72	0.42	1.17	8.31	−0.31	−0.22	3.08	4.75
	Cu	9.79	0.80	0.23	10.82	0.18		3.80	5.22
$[Fe_3(CO)_{12}Cu_4(P(CH_3)_3)_2]^{2-}$ (IV)	Fe(1)	6.70	0.42	1.22	8.34	−0.33	−0.19	3.08	4.76
	Fe(2,3)	6.71	0.42	1.17	8.30	−0.30	−0.21	3.09	4.76
	Cu(1)	9.84	0.73	0.47	11.04	−0.03		3.68	5.17
	Cu(2,3)	9.79	0.79	0.21	10.79	0.21		3.80	5.22
$((C_6H_{11})_3PCu)_2Fe(CO)_4$ (V)	Fe	6.73	0.42	1.10	8.25	−0.25	−0.13	3.09	4.74
	Cu	9.84	0.80	0.38	11.02	−0.03		3.70	5.17
$((Ph_3P)_2Cu)_2Fe(CO)_4$ (VI)	Fe	6.76	0.41	1.05	8.22	−0.22	−0.22	3.09	4.72
	Cu	9.84	0.60	0.75	11.19	−0.18		3.57	5.15
$(Ph_3P)_2CuFe(CO)_3(NO)$ (VII)	Fe	6.69	0.41	1.31	8.41	−0.41	−0.08	3.06	4.77
	Cu	9.85	0.62	0.74	11.21	−0.22		3.57	5.14

[a] The Slater [23,24] effective nuclear charge experienced by the metal 4s electrons. [b] The Clementi and Raimondi [24] effective nuclear charge experienced by the metal 4s electrons.

site and, in each case, the Mössbauer spectra of these molecules were successfully fit with one symmetric quadrupole doublet.

3.2. Fenske–Hall molecular orbital calculations

Fenske–Hall molecular orbital calculations, the clusters have been carried out to provide a better picture of the electron distribution in these clusters and to determine how these distributions are reflected in the Mössbauer effect spectral parameters. The detailed molecular orbital energy diagrams, wave functions, and overlap populations are presented elsewhere [17]. The results of the energy calculations defined above are given in Table 2. The metal Mulliken atomic populations, charges, and effective nuclear charges are given in Table 3.

The molecular orbital energy level diagrams of the anionic clusters are distinctly different from those of the neutral molecules. The diagrams of the anionic clusters lie between those of pure bulk metals or alloys and discrete molecules and show a "band-like" structure in which the lower energy molecular orbital bands are comprised solely of either $[Fe(CO)_4]^{2-}$ or copper fragment orbitals. In contrast, the molecular orbital diagrams of the neutral compounds show more interaction of these lower $[Fe(CO)_4]^{2-}$ orbitals and the copper fragment orbitals.

A molecular orbital diagram of the frontier orbitals of a typical $[Fe(CO)_4]^{2-}$ fragment is shown in Fig. 4(A). Although not shown in Fig. 4(A), the molecular orbitals found between -20 and -30 eV, where the carbon–oxygen bonding occurs, contain carbon and oxygen 2s and 2p atomic orbital character [17]. The iron–carbon bonding occurs in the molecular orbitals found between 8 and -11 eV. The greatest overlap occurs between the iron 4p and the carbon 2p atomic orbitals. A closer look at the Mulliken atomic populations of the $[Fe(CO)_4]^{2-}$ fragments show that formation of the $[Fe(CO)_4]^{2-}$ fragment orbitals, from iron atomic orbitals and carbonyl fragment orbitals, causes the iron 3d atomic orbitals to lose electrons and the iron 4s and 4p atomic orbitals to gain electrons. This change is reflected in the valence electronic configuration of the iron atom which starts out as $4s^0 3d^8 4p^0$ and becomes, on average, $4s^{0.4} 3d^{6.6} 4p^{1.3}$, upon formation of $[Fe(CO)_4]^{2-}$.

Because the composition of the molecular orbitals of each anionic cluster studied in this work is similar, only the molecular orbital diagram of the frontier orbitals of $[Cu_3Fe_3(CO)_{12}]^{3-}$ (Fig. 4(B)), is discussed in detail. The bonding molecular orbitals found between -5 and -50 eV are formed completely from $[Fe(CO)_4]^{2-}$ fragment orbitals and contain predominately carbon and oxygen 2s and 2p atomic orbital character. Although not shown in Fig. 4(B), those molecular orbitals lying below -25 eV have virtually no iron atomic orbital character and represent localized carbonyl bonding. Those found between -10 and -13 eV have some iron 4s atomic orbital character, whereas those between -5 and -7 eV contain mainly iron 3d and a small amount of iron 4p atomic orbital character. The nonbonding molecular orbitals between -1 and -3 eV contain only $[Cu_3]^{3+}$ fragment orbitals and contain predominately copper 3d atomic orbital character. The molecular orbitals near and including the HOMO, the frontier orbitals, are a combination of

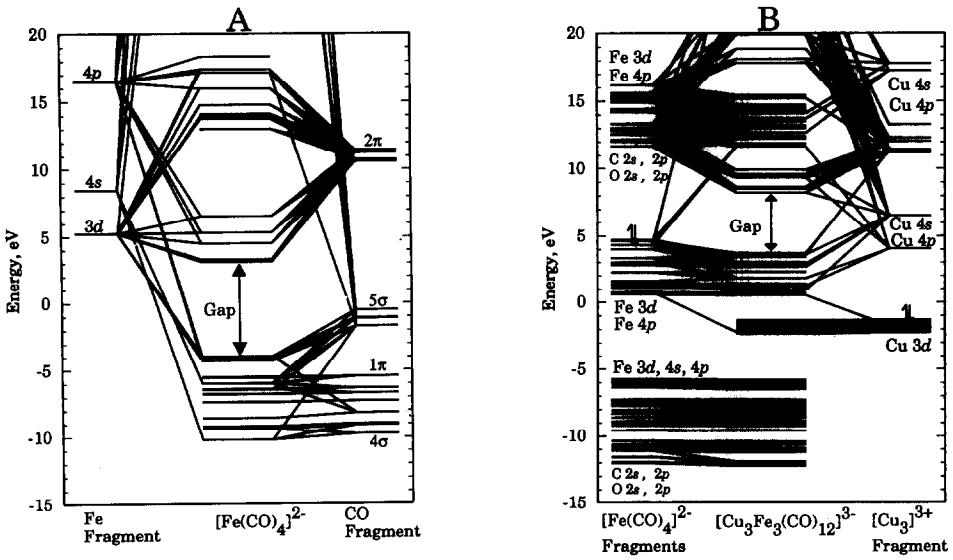

Fig. 4. Molecular orbital diagram of the frontier orbitals of the $[Fe(CO)_4]^{2-}$ fragment (A) and $[Cu_3Fe_3(CO)_{12}]^{3-}$ cluster (B).

occupied $[Fe(CO)_4]^{2-}$ fragment orbitals and unoccupied $[Cu_3]^{3+}$ fragment orbitals. The occupied $[Fe(CO)_4]^{2-}$ fragment orbitals act as donor orbitals, overlapping with the unoccupied $[Cu_3]^{3+}$ fragment acceptor orbitals. A closer look [17] at the frontier orbitals, shows that the occupied iron 3d and 4p atomic orbitals overlap with the copper 4s and 4p atomic orbitals. The overlap populations between the iron 3d and 4p atomic orbitals and the copper 4s and 4p atomic orbitals are large and positive, indicating the presence of a strong iron–copper bond. This is the major iron–copper bonding in these anionic clusters. The copper–copper bonding occurs near the HOMO. Even though there is some copper-copper bonding between -1 and -3 eV which involves copper 3d and 4s atomic orbitals, the major copper–copper bonding involves the copper 4s and 4p atomic orbitals found between zero and 5 eV. The unoccupied $[Cu_3]^{3+}$ fragment orbitals form occupied molecular orbitals upon formation of the cluster.

The overlap populations [17] between metal atoms in the anionic clusters show that the major metal–metal bonding is between the iron and copper atoms. The copper–copper overlap populations are positive, indicating the presence of copper–copper bonds. However, because the typical copper–copper bond distances are longer, the copper–copper overlap populations are much smaller than the iron–copper overlap populations, and as a result, the copper–copper bonds are weaker. In these copper–iron clusters, the $Fe(CO)_4$ groups, which cap the copper moiety, hold the cluster together with strong iron–copper bonds.

Unlike the molecular orbital diagrams of the anionic clusters, **I–III**, the molecular orbital diagram of $[Fe_3(CO)_{12}Cu_4(P(CH_3)_3)_2]^{2-}$ (**IV**) [17] has several groups of bonding molecular orbitals below the HOMO which are formed completely from $[Cu_4(P(CH_3)_3)_2]^{4+}$ fragment orbitals. The molecular orbitals found between -15 and -30 eV do not contain any copper atomic orbital character, but rather they contain the atomic orbitals of the $P(CH_3)_3$ ligands. Although the molecular orbitals found between -9 and -15 eV show some overlap between the $[Fe(CO)_4]^{2-}$ and $[Cu_4(P(CH_3)_3)_2]^{4+}$ fragment orbitals, the only bonding between the $[Fe(CO)_4]^{2-}$ and $[Cu_4(P(CH_3)_3)_2]^{4+}$ fragment orbitals in this region, occurs through the copper 4s atomic orbital overlap with the carbon 2p atomic orbital.

The distribution of atomic orbitals in the molecular orbital diagrams of the neutral molecules is similar to that found in the molecular orbital diagrams of the anionic clusters, and are discussed in detail elsewhere [17]. The discrete groups of molecular orbitals, which are formed completely from $[Fe(CO)_4]^{2-}$ or copper fragment orbitals, are not as apparent in the molecular orbital diagrams of these neutral molecules. The iron–copper bonding in the neutral molecules is very similar to that found in the anionic clusters. As in the anionic clusters, the iron–copper bonding in these neutral molecules occurs near and including the HOMO where the occupied $[Fe(CO)_4]^{2-}$ fragment orbitals overlap with the unoccupied $[Cu(PPh_3)_2]^{+}$ fragment orbitals. These bonding frontier orbitals are predominately iron 3d and 4p and copper 4s and 4p atomic orbitals. There is no copper–copper bonding in the neutral molecules. The copper–copper distance in $((C_6H_{11})_3PCu)_2Fe(CO)_4$ (**V**) is 2.97 Å, and is 0.3 Å larger than the average copper–copper bond distance found in the anionic clusters. It is also larger than the van der Waals copper–copper contact distance of 2.86 Å [21]. The results of the molecular orbital calculations show, as expected, that the copper–copper atomic overlap populations for this molecule are small and slightly negative, indicating that no bonding exists between the two copper atoms.

The electronic distribution within these clusters may be further understood by examining their Mulliken atomic charges. The average ligand and metal charges are shown in Fig. 5. The phosphine-like and carbonyl ligands in these clusters are Lewis bases, donating electron density to the metal atoms. It is the phosphorus atom of the phosphine-like ligand which is donating electron density to the copper atom. Likewise, the carbon atom of the carbonyl ligand is donating electron density to the iron atom.

The phosphine-like ligand phosphorus charge becomes more positive as it donates additional electron density to the copper atom, which in turn become more negative. These trends, shown in Fig. 5, are seen in the neutral clusters. The number of phosphine-like ligands also influences the copper charge. The copper charge of cluster **V**, which has only one phosphine-like ligand, is considerably more positive than the copper in **VI** and **VII** each of which have two phosphine-like ligands per copper atom. Both phosphine-like ligand phosphorus atoms donate electron density to the copper atom which then has a more negative charge. The most positive phosphine-like ligand phosphorus charge is found in the dianionic cluster, $[Fe_3(CO)_{12}Cu_4(P(CH_3)_3)_2]^{2-}$ (**IV**). Even though, in this cluster, the Cu(1) charge, which has one phosphine-like ligand is, as expected, more negative than those of Cu(2,3), which have no phosphine-like ligands, it is not as negative as the copper charges found in the neutral clusters. This higher copper charge may be explained by the differences in the copper bonding of the neutral and dianionic clusters. In both the neutral clusters and cluster **IV**, the copper atoms are accepting electron density

from the phosphine-like ligands, and because copper is more electronegative than iron, the copper atoms are also withdrawing electron density from the iron atoms. However, the copper–copper overlap populations in cluster **IV** show that the copper atoms are also sharing electron density with their copper neighbors, a situation that does not exist in the neutral clusters. This delocalization of copper electron density yields the more positive observed copper charge.

The average carbonyl ligand carbon charge becomes more positive as it donates more electron density to the iron atom whose charge in turn will become more negative. These trends are also observed in Fig. 5 for the neutral clusters. However, these trends are not seen in the anionic clusters. The structures of the anionic clusters may explain the rather constant carbonyl ligand charges and the varying iron charges, which are shown in Fig. 5. The most positive iron charges correspond to those iron atoms which have the

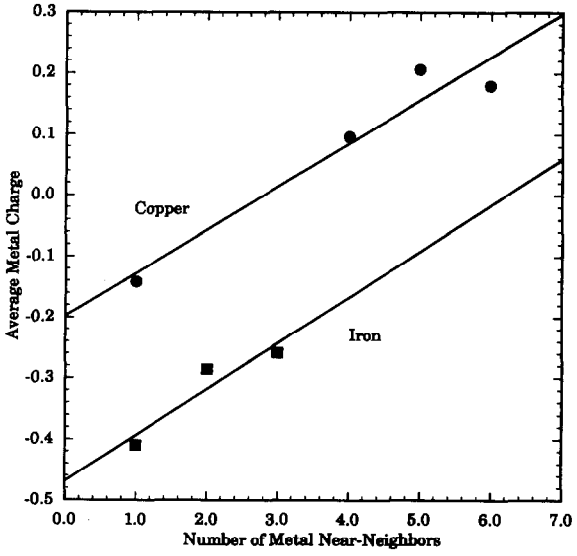

Fig. 6. The number of metal near-neighbors versus the average iron charge (■), and the average copper charge (●).

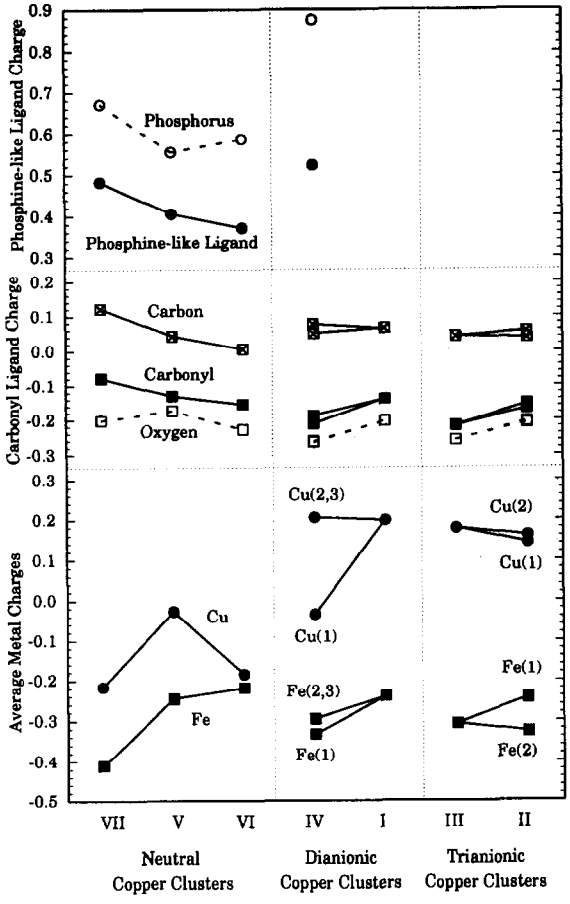

Fig. 5. The average phosphine-like ligand phosphorus charge (○), the average phosphine-like ligand charge (●). The average carbonyl ligand carbon charge (⊠), the average carbonyl ligand charge, (■), and the average carbonyl ligand oxygen charge (□). The average copper charge (●), and the average iron charge (■).

largest number of near-neighbor copper atoms, near-neighbors that create more delocalization of the iron electron density and thus a more positive iron charge. The linear increase in the charge of a metal atom, as a result of delocalization of the metal electron density onto its near-neighbor cluster atoms, is shown in Fig. 6. Both the iron and copper charge give a slope of 0.07 electrons per near-neighbor.

The iron and copper Mulliken atomic orbital populations for the clusters are shown in Fig. 7 and Table 3, respectively. The iron 4s atomic orbital populations are virtually constant and the iron 3d atomic orbital populations have similar values in these clusters. In contrast, the iron 4p atomic orbital populations have a large range of values. Further, the copper 4s atomic orbital populations are similar and the copper 3d atomic orbital populations are virtually constant in these clusters. However, as with the iron populations, it is the copper 4p atomic orbital populations which show the greatest range of values. Because the Mulliken atomic orbital populations are calculated from the overlap populations, the orbitals whose populations are similar also have a small range of overlap populations. Likewise, the iron and copper 4p atomic orbitals have the greatest range of overlap populations. Iron overlap populations indicate that the iron atoms of cluster **VII** accept more electron density from a nitrosyl ligand nitrogen atom or from a carbonyl ligand carbon atom than do the iron atoms of the other neutral clusters, **V** and **VI**. The additional electron density is found in the iron 4p atomic orbitals of cluster **VII**. The differences in the copper near-neighbor environment of the neutral clusters provide an explanation for the differences

observed in the copper atomic orbital populations. As mentioned above, cluster **V** has only one phosphine-like ligand, whereas clusters **VI** and **VII** have two phosphine-like ligands. The additional electron density provided to the copper atom by the second phosphine-like ligand phosphorus atom is found in the copper 4p atomic orbital populations of clusters **VI** and **VII**. The orbitals whose populations show the greatest range of values, the iron 3d and 4p and the copper 4s and 4p orbitals, are also the orbitals near the HOMO where most of the metal-metal bonding occurs.

The energy of the occupied molecular orbitals, E_T, and the cluster bond energy, E_{BE}, as defined above, as well as the HOMO-LUMO gap energy, and the average metal-metal bond distances, are given in Table 2. In this table, a positive value of E_{BE} represents the energy required to break an iron–copper bond. Our calculations [17] reveal that, as expected, more energy is required to break shorter, stronger iron–copper bonds, a conclusion that is in agreement with the iron–copper overlap populations mentioned above. Our calculations [17] also reveal that the HOMO–LUMO gap increases almost linearly as the average iron–copper bond distance decreases with a slope of −0.05 Å per eV, an intercept of 2.65 Å, and a correlation coefficient of 0.95. As expected, a larger HOMO–LUMO gap corresponds to a shorter, stronger, average iron–copper bond distance and hence a more stable cluster.

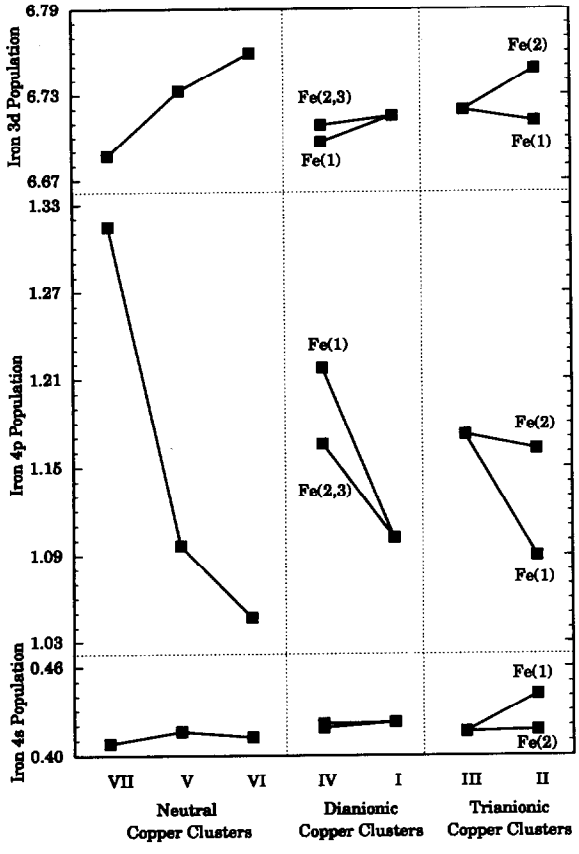

Fig. 7. The iron Mulliken atomic orbital populations.

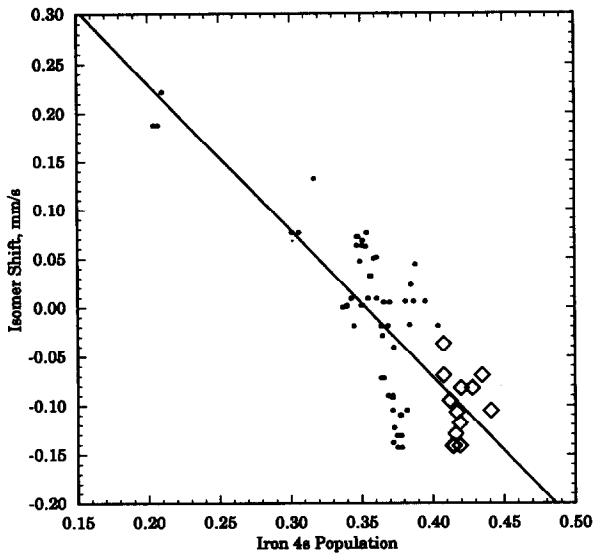

Fig. 8. The isomer shift versus the iron 4s Mulliken atomic population for the iron–copper clusters (◇). The small points represent values obtained for a variety of related organoiron clusters, see text for references.

3.3. Mössbauer effect isomer shifts

The results of the Fenske–Hall molecular orbital calculations, given in Table 3, may be used to both better understand the differences observed in the isomer shifts in these and related clusters and to support the assignment of the components of the Mössbauer spectrum of $Na_3[Cu_5Fe_4(CO)_{16}]$ (**II**). It is well known that, as the s-electron density at the iron nucleus increases, the isomer shift decreases [22]. The s-electron density at the iron nucleus is proportional to the iron 4s Mulliken atomic orbital population and the effective nuclear charge it experiences, both of which can be obtained from the Fenske–Hall molecular orbital calculations. This linear relationship between the isomer shift and the 4s Mulliken atomic population, which has a slope of −1.50 mm/s per electron, an intercept of 0.53 mm/s and a correlation coefficient of 0.81, is shown in Fig. 8. The small range of the iron 4s Mulliken atomic populations found in these iron–copper clusters indicates that the presence of a copper serves to create a similar "ideal" electronic environment at the iron sites. In these clusters, this ideal environment has a configuration which ranges from $4s^{0.41}3d^{6.76}4p^{1.05}$ in **VI**, to $4s^{0.41}3d^{6.69}4p^{1.31}$ in **VII**, with an average configuration of $4s^{0.42}3d^{6.72}4p^{1.15}$. The simi-

larity of the iron near-neighbor environments provided by the four carbonyl ligands bonded to each iron, also contributes to the small range of electronic environments and hence of isomer shifts.

The 4s Mulliken atomic populations do not take into account the shielding of the 4s electrons by the 3d and 4p electrons. As the effective nuclear charge experienced by the iron 4s electrons increases, the 4s radial electronic distribution decreases, the s-electron density at the iron nucleus increases, and, consequently, the isomer shift decreases. The Slater effective nuclear charges, Z_{eff}, experienced by the iron 4s electrons were calculated [23,24] from the iron Mulliken atomic populations and are included in Table 3. However, as indicated earlier [3,11], the more modern Clementi and Raimondi [24] effective nuclear charges are more useful in understanding the isomer shifts. In this approach, Clementi and Raimondi used self-consistent field wave functions to obtain the shielding experienced by an electron. The Clementi and Raimondi effective nuclear charge experienced by the 4s electrons is also included in Table 3. The Clementi and Raimondi effective nuclear charge experienced by a free isolated iron 4s electron in the $4s^2 3d^6 4p^0$ electronic configuration is 5.434 [24]. The average effective nuclear charge experienced by the iron 4s electrons in the iron–copper clusters studied here is 4.75, a value considerably smaller than in the isolated iron atom. The iron–copper and the iron to carbonyl ligand bonding in these clusters increased the iron 3d and 4p atomic orbital populations and decreased the iron 4s atomic orbital population, thereby leading to a larger screening constant for the iron 4s electrons and a smaller effective nuclear charge.

A better representation of the s-electron density at the iron nucleus may be obtained by considering both the iron 4s Mulliken atomic orbital population and the effective nuclear charge experienced by the iron 4s electrons. The correlation between the observed isomer shift and the iron 4s Mulliken atomic population plus the Clementi and Raimondi effective nuclear charge is shown in Fig. 9, which also includes values

TABLE 4. A comparison of observed and calculated cluster electric field gradients [a]

Cluster	Site	Obs. ΔE_Q	Calc. total			Calc. valence					Calc. lattice			
			ΔE_Q	V_{zz}	η	ΔE_Q	V_{zz}	η	$\langle r^{-3} \rangle$	%	ΔE_Q	V_{zz} [b]	η	%
$Na_2[Cu_6Fe_4(CO)_{16}]$ (I)	Fe(1)	0.617	0.39	0.19	0.01	0.36	0.17	0.01	31.6	92	0.03	0.02	0.00	8
	Fe(2)	0.617	0.62	0.28	0.58	0.61	0.28	0.57	31.4	99	0.03	0.01	0.31	1
	Cu(1)	–	–	0.06	0.89	–	0.06	0.85	32.0	–	–	0.01	0.52	–
	Cu(2)	–	–	0.05	0.98	–	−0.06	0.96	32.0	–	–	0.01	0.69	–
$Na_3[Cu_5Fe_4(CO)_{16}]$ (II)	Fe(1)	0.683	0.67	0.31	0.41	0.67	0.31	0.39	31.5	99	−0.01	−0.01	0.36	1
	Fe(2)	0.472	−0.07	−0.03	0.89	0.06	0.02	0.82	31.3	86	−0.01	−0.01	0.21	14
	Cu(1)	–	–	−0.10	0.69	–	−0.10	0.61	32.0	–	–	−0.01	0.65	–
	Cu(2)	–	–	−0.10	0.12	–	−0.10	0.26	32.0	–	–	0.01	0.57	–
$Na_3[Cu_3Fe_3(CO)_{12}]$ (III)	Fe(1)	0.442	1.36	0.62	0.54	1.35	0.62	0.55	31.4	99	0.02	0.01	0.48	1
	Fe(2)	0.442	1.47	0.67	0.54	1.46	0.67	0.55	31.5	99	0.02	0.01	0.51	1
	Fe(3)	0.442	−0.73	−0.32	0.80	−0.72	−0.32	0.78	31.3	99	0.01	0.01	0.60	1
	Cu(1)	–	–	−0.12	0.95	–	−0.13	0.83	32.0	–	–	−0.01	0.76	–
	Cu(2)	–	–	0.11	0.37	–	0.10	0.36	32.0	–	–	−0.01	0.88	–
	Cu(3)	–	–	−0.14	0.75	–	−0.14	0.66	32.0	–	–	−0.01	0.88	–
$[Cu(P(CH_3)_3)_4]_2$-	Fe(1)	0.200	−1.10	−0.53	0.05	−1.10	−0.53	0.25	31.5	99	−0.02	−0.01	0.94	1
$[Fe_3(CO)_{12}Cu_4$-	Fe(2)	0.815	1.65	0.75	0.59	1.65	0.76	0.57	31.2	99	0.01	0.01	0.36	1
$(P(CH_3)_3)_2]$ (IV)	Fe(3)	0.815	1.01	0.45	0.70	1.01	0.45	0.72	31.7	99	0.02	0.01	0.37	1
	Cu(1)	–	–	−0.13	0.81	–	−0.11	0.89	32.0	–	–	0.02	0.33	–
	Cu(2)	–	–	0.09	0.71	–	0.09	0.68	32.0	–	–	−0.01	0.85	–
	Cu(3)	–	–	0.14	0.67	–	0.13	0.62	32.0	–	–	−0.01	0.73	–
$((C_6H_{11})_3PCu)_2Fe(CO)_4$	Fe	0.192	−0.60	−0.26	0.81	−0.60	−0.26	0.80	31.4	99	−0.01	−0.01	0.47	1
(V)	Cu(1)	–	–	0.10	0.54	–	0.09	0.66	32.0	–	–	0.01	0.42	–
	Cu(2)	–	–	0.10	0.82	–	0.09	0.95	32.0	–	–	0.01	0.39	–
$((Ph_3P)_2Cu)_2Fe(CO)_4$	Fe	2.497	−1.06	−0.51	0.16	−1.05	−0.50	0.17	31.3	99	−0.01	−0.01	0.88	1
(VI)	Cu(1)	–	–	0.27	0.26	–	0.27	0.22	32.0	–	–	0.02	0.39	–
	Cu(2)	–	–	0.23	0.20	–	0.22	0.27	32.0	–	–	0.02	0.40	–
$(Ph_3P)_2CuFe(CO)_3(NO)$	Fe	0.262	−1.45	0.68	0.32	−1.45	−0.68	0.32	31.7	99	0.02	0.01	0.33	1
(VII)	Cu	–	–	0.29	0.33	–	0.30	0.42	32.0	–	–	0.02	0.26	–

[a] The ΔE_Q values have the units of mm/s and the V_{zz} values must be multiplied by 10^{22} V/m^2. The observed ΔE_Q values were obtained at 78K.

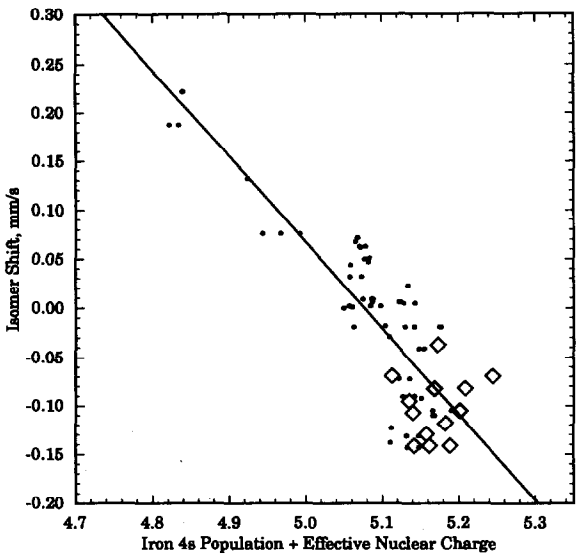

Fig. 9. The isomer shift versus the 4s Mulliken atomic population plus the Clementi and Raimondi effective nuclear charge for the iron–copper clusters (◇). The small points represent values obtained for a variety of related organoiron clusters, see text for references.

from our work on related iron clusters [2,3,8–12]. This plot has a slope of −0.88 mm/s per electron, an intercept of 4.47 mm/s and a correlation coefficient of 0.86. Although both the range of isomer shifts and values of the iron 4s Mulliken atomic orbital population plus the Clementi and Raimondi effective nuclear charge are small, their values do correlate well with those observed in our work on related organoiron clusters [2,3,8–12].

As mentioned in the Introduction, organometallic clusters are often used as models for the metal surfaces in metals or alloys and it is interesting to compare the isomer shifts observed in copper–iron alloys with those of the clusters studied here. The room temperature Mössbauer spectrum of a copper–iron alloy has several components [25–28] which include a magnetic sextet, corresponding to α-iron, a singlet with an isomer shift of −0.1 mm/s, corresponding to γ-iron, and up to three doublets corresponding to isolated iron clusters in a solid solution of copper. For clusters with approximately two iron atoms the isomer shift is in the −0.03 to −0.06 mm/s range. As the iron cluster increases in size, the isomer shift decreases to −0.12 to −0.16 mm/s for four to five iron atom clusters and to *ca.* −0.21 mm/s for six to seven iron atom clusters. The negative room temperature isomer shifts observed for these doublets are very similar to the room temperature isomer shifts observed for clusters **I**, **II**, **III**, given in Table 1, and indicate the very similar metal–metal bonding found in the alloy clusters and in the organoiron–copper clusters.

3.4. Mössbauer effect quadrupole interaction

The valence and lattice contributions to the iron and copper electric field gradients, calculated from the molecular orbital wave function coefficients and the Mulliken atomic charges, respectively, are given in Table 4. It is clear that the major contribution to the electric field gradient in these clusters is the valence contribution. The nonintegral, non equivalent atomic populations of the iron and copper 3d and 4p atomic orbitals lead to the dominance of the valence contribution over the lattice contribution to the electric field gradient.

Support of the assignment of the two components in the Mössbauer spectrum of **II** is found in the electric field gradient calculations. The calculated electric field gradients for this cluster yield two significantly different quadrupole splittings. The calculated quadrupole splitting of 0.67 mm/s for Fe(1) is similar to the experimental value of 0.683 mm/s for the outer quadrupole doublet. Both the calculated and experimental quadrupole splittings for Fe(2), −0.07 mm/s and 0.472 mm/s, respectively, are smaller than the values for the Fe(1) site. The significantly different calculated quadrupole splittings confirm the assignment of the Mössbauer effect spectrum of cluster **II** given in Table 1.

The experimental values of ΔE_Q are compared with the calculated values of ΔE_Q in Fig. 10, where data for several related series of organoiron clusters [2,3,8–12]

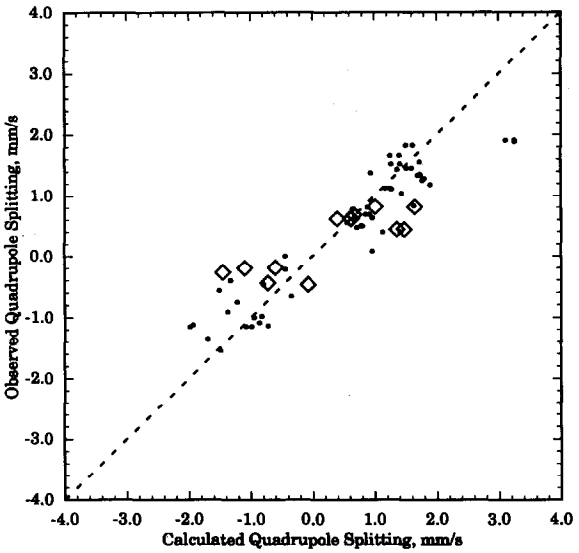

Fig. 10. The observed Mössbauer effect quadrupole splittings versus the quadrupole splitting obtained from the electric field gradients calculated from the iron molecular orbital wave functions and the atomic charges for the iron–copper clusters (◇). The small points represent values obtained for a variety of related organoiron clusters, see text for references.

are also shown. Because the experimental Mössbauer spectra yield only the magnitude of ΔE_Q, the sign of the calculated value of ΔE_Q was assigned to the experimental value of ΔE_Q. Figure 10 indicates that the Fenske–Hall molecular orbital calculations are useful in predicting the electric field gradients in clusters, especially those that contain only iron [2,3,8–12]. There is poorer agreement between the observed and calculated values of ΔE_Q for the mixed metal iron–copper clusters. There are several possible explanations for this disagreement. One possibility is that the γ and R Sternheimer factors [29,30], should be included in the calculated value of the electric field gradient. These factors account for the polarization of the symmetric electronic core distribution by the nonspherical lattice and valence electronic distributions. Because the lattice contribution is small, a negligible Sternheimer anti shielding factor, γ, is expected. In clusters such as **III**, **IV**, and **VII**, in which the calculated ΔE_Q is greater than the observed ΔE_Q, the Sternheimer shielding factor, R, will serve to reduce the overall electric field gradient and hence the calculated value of ΔE_Q. Another possible explanation for the disagreement between the observed and calculated values of ΔE_Q for the mixed metal iron–copper clusters is that the X-ray crystal structure used for the molecular orbital calculations, and thus the electric field gradient calculations, was not always the structure for the specific compound measured in the Mössbauer effect study. For example, the Mössbauer spectra were measured for $Na_3[Cu_5Fe_4(CO)_{16}]$ (**II**) and $Na_3[Cu_3Fe_3(CO)_{12}]$ (**III**), the sodium salt, but the X-ray structure was obtained for the tetraethylammonium salt. Also, for the neutral clusters **V** and **VI**, the structure was an approximation of the X-ray crystal structure. In related studies [9,17], we have found that small changes in the metal–metal bond distance of 0.02 Å changed the molecular orbital wave function coefficients and in turn the resulting electric field gradients by up to 15%. Finally, the disagreement between the observed and the calculated values of ΔE_Q may be a result of our use of "nonideal" atomic basis functions, especially for the metal atoms.

Table 4 shows that, within a given cluster, iron sites that are chemically equivalent although crystallographically inequivalent, may have rather different electric field gradients. These differences, although not resolved in the Mössbauer spectra of the clusters, can be related to the structure of the clusters. The quadrupole splitting, ΔE_Q, is a measure of the deviation in the electronic distribution at the iron site from perfect cubic symmetry. The ligands of the iron atoms in the iron–copper clusters can have either a six-coordinated octahedral or a seven-coordinate pentagonal bipyramidal structure. A six-coordinated iron site may be represented by an octahedron in which all the angles are 90°. The ideal seven-coordinate complex could be represented as a pentagonal bipyramid with all 90° and 72° angles. These are the optimum angles given in Table 5. This table reveals that within a cluster, the site that deviates most from octahedral or pentagonal bipyramidal symmetry has, as expected, the largest calculated electric field gradient and hence ΔE_Q. For example, in cluster **III**, the bonding environment about the Fe(2) site deviates the most from octahedral symmetry, whereas that about the Fe(3) site deviates the least. Table 5 also indicates that in cluster **III**, these sites have the largest and smallest calculated values of ΔE_Q, respectively.

4. Conclusions

This study has shown that the Mössbauer effect isomer shift and the quadrupole interaction are extremely sensitive to the changes in the electronic envi-

TABLE 5. Comparison of structure with perfect octahedral geometry

Cluster	Site	Obs. ΔE_Q [a]	Calc. ΔE_Q [a]	Coordination Number	Optimum angle	Avg. angle	Difference in angle	Range of site-NN distances, (Å)
$Na_3[Cu_5Fe_4(CO)_{16}]$ (II)	Fe(1)	0.683	0.67	7	72	71.9	0.1	0.76
					90	87.2	2.8	
					180	137.6	42.4	
	Fe(2)	0.472	−0.07	6	90	88.1	1.9	0.64
					180	150.9	29.1	
$Na_3[Cu_3Fe_3(CO)_{12}]$ (III)	Fe(1)	0.442	1.36	6	90	91.1	1.1	0.70
					180	136.9	43.1	
	Fe(2)	0.442	1.47	6	90	92.1	2.1	0.73
					180	133.1	46.9	
	Fe(3)	0.422	−0.73	6	90	89.1	0.9	0.68
					180	147.7	32.3	

[a] The ΔE_Q values have the units of mm/s.

ronment of an iron nucleus. These changes were successfully correlated to the results of theoretical Fenske–Hall molecular orbital calculations. The iron 4s Mulliken atomic populations in these clusters were found to be very similar. The isomer shift was found to be best represented by the sum of the iron 4s Mulliken atomic population and the Clementi and Raimondi effective nuclear charge experienced by the iron 4s electrons. The Mössbauer effect quadrupole splittings were rather successfully calculated by using the results of the Fenske–Hall molecular orbital calculations. The major contribution to the electric field gradient is the valence contribution.

The results of the Fenske–Hall molecular orbital calculations show that the iron carbonyl groups hold the clusters together by producing strong iron–copper bonds, bonds which are stronger than the copper–copper bonds. The phosphine and carbonyl ligand charges were found to become more positive as these Lewis bases donated electrons to the metal atoms whose charges then became more negative. There is an approximately linear relationship between the metal charges and the number of metal near-neighbors. The copper charge of the neutral clusters was found to become more negative as the number of phosphine-like ligands increased.

Acknowledgements

The authors thank Dr. M.B. Hall of Texas A&M University for the FENSKE–HALL program. We thank Drs. J.F. O'Brien, F. Grandjean, G. Bertrand, A. Penico, and D.E. Tharp for many helpful discussions. The authors also thank the donors of the Petroleum Research Fund, administered by the American Chemical Society, for their financial support of this work.

References and notes

1 E.L. Muetterties, T.N. Rhodin, E. Band, C.F. Brucker and W.R. Pretzer, *Chem. Rev., 79* (1979) 91.
2 C.G. Benson, G.J. Long, J.W. Kolis and D.F. Shriver, *J. Am. Chem. Soc., 107* (1985) 5297.
3 C.G. Benson, G.J. Long, J.S. Bradley, J.W. Kolis and D.F. Shriver, *J. Am. Chem. Soc., 108* (1986) 1898.
4 G. Doyle, B.T. Heaton and E. Occhiello, *Organometallics, 4* (1985) 1224.
5 G. Doyle, K. A. Eriksen and D. Van Engen, *J. Am. Chem. Soc., 108* (1986) 445.
6 G. Doyle, K. A. Eriksen and D. Van Engen, in K.D. Karlin and J. Zubieta (eds.,) *Biological and Inorganic Copper Chemistry*, Vol. 2, Adenine Press, New York, 1985, p. 243.
7 G. Doyle, K.A. Eriksen and D. Van Engen, *J. Am. Chem. Soc., 107* (1985) 7914.
8 M.L. Buhl, G.J. Long and J.F. O'Brien, *Organometallics, 12* (1993) 283.
9 M.L. Buhl, G.J. Long and J.F. O'Brien, *Organometallics, 12* (1993) 1902.
10 M.L. Buhl and G.J. Long, *J. Organomet. Chem., 461* (1993) 177.
11 G.J.Long and J.F. O'Brien, *Hyperfine Interactions, 40* (1988) 101.
12 M.B. Hall and R.F. Fenske, *Inorg. Chem., 11* (1972) 768.
13 Because of the presence of triphenylphosphine ligands in $[(Ph_3P)_2CuFe(CO)_3(NO)]$ (VII) the total number of valence and virtual atomic orbitals exceeded the dimensions of the FENSKE–HALL program [17]. To overcome this limitation, the phenyl groups were replaced by hydrogens at a distance of 1.48 Å from the phosphorus. In $[((C_6H_{11})_3PCu)_2Fe(CO)_4]$ (V), the cyclohexyl groups in the tricyclohexyl-phosphine ligands were replaced by hydrogen, again at a distance of 1.48 Å from the phosphorous. The influence on such substitutions of the Fenske–Hall calculations has been investigated [17] and found to have a negligible effect on the molecular orbital results.
14 F. Herman and S. Skillman, *Atomic Structure Calculations*, Prentice Hall, Englewood Cliffs, NJ, 1963.
15 (a) B.E. Bursten and R.F. Fenske, *J. Chem. Phys., 67* (1977) 3138; (b) B.E. Bursten, R.J. Jensen and R.F. Fenske, *J. Chem. Phys., 68* (1978) 3320.
16 See instructions provided with the Fenske–Hall code.
17 M.L. Buhl, *PhD Thesis*, University of Missouri-Rolla, Rolla, MO, 1993.
18 A. Trautwein, F.E. Harris and I. Dezsi, *Theor. Chim. Acta (Berlin), 35* (1974) 231.
19 J.L.K F. De Vries, C.P. Keijzers and E. De Boer, *Inorg. Chem., 11* (1972) 1343.
20 M. Weissbluth and J.E. Maling, *J. Chem. Phys., 47* (1967) 4166.
21 W.W. Porterfield, *Inorganic Chemistry: A Unified Approach*, Addison-Wesley, Reading, MA, 1984, p 168.
22 G.K. Shenoy, in: G.J. Long (ed.), *Mössbauer Spectroscopy Applied to Inorganic Chemistry*, Vol.1, Plenum Press, New York, 1984, p 57.
23 J.C. Slater, *Phys. Rev., 36* (1930) 57.
24 J.E. Huheey, *Inorganic Chemistry: Principles of Structure and Reactivity*, 3rd edition, Harper and Row, New York, 1983, pp. 37–38.
25 P.E. Clark, J.M. Cadogan, M.J. Yazxhi and S.J. Campbell, *J. Phys. F: Metal Phys., 9* (1979) 379.
26 S.J. Campbell, P.E. Clark and P.R. Liddell, *J. Phys. F: Metal Phys., 2* (1972) L114.
27 U. Herr, J. Jing, U. Gonser and H. Gleiter, *Solid State Commun., 76* (1990) 197.
28 S.J. Campbell and P.E. Clark, *J. Phys. F: Metal Phys., 4* (1974) 1073.
29 R. Ingalls, *Phys. Rev., 133* (1964) A787.
30 N.N. Greenwood and T.C. Gibb, *Mössbauer Spectroscopy*, Chapman and Hall, London, 1974, p. 49.